Title

Adaptive optics-optical coherence tomography for in vivo retinal imaging: comparative analysis of two wavefront correctors

Journal

COHERENCE DOMAIN OPTICAL METHODS AND OPTICAL COHERENCE TOMOGRAPHY IN BIOMEDICINE X, 6079

ISSN

0277-786X

Authors

Zawadzki, RJ
Jones, SM
Zhao, M
et al.

Publication Date

2006

DOI

10.1117/12.647568

Peer reviewed

Adaptive optics - optical coherence tomography for in vivo retinal imaging: comparative analysis of two wavefront correctors

Robert J. Zawadzki*[a], Steven M. Jones[b], Mingtao Zhao[c], Stacey S. Choi[a], Sophie S. Laut[a], Scot S. Olivier[b], Joseph A. Izatt[c] and John S. Werner[a]

[a] Vision Science and Advanced Retinal Imaging Laboratory, Dept. of Ophthalmology & Vision Science, UC Davis, 4860 Y Street, Suite 2400, Sacramento, CA, USA 95817;
[b] Lawrence Livermore National Laboratory, 700 East Avenue, Livermore, CA, USA 74550;
[c] Department of Biomedical Engineering, Duke University, 101 Science Drive, Durham, North Carolina 27708;

ABSTRACT

Adaptive optics - optical coherence tomography (AO-OCT) has the potential to improve lateral resolution for OCT retinal imaging. Several reports have already described the successful combination of AO with a scanning confocal Fourier-domain OCT instrument to permit real-time three-dimensional (3D) imaging with high resolution (in all three dimensions). One of the key components that sets the performance limit of AO is the wavefront corrector. Several different wavefront correctors have been used in AO-OCT systems so far. In this paper we compare two commercially available wavefront correctors: an AOptix Bimorph deformable mirror (DM) and a Boston Micromachines Micro-Electro Mechanical System (MEMS) DM (used for the first time in an AO-OCT system). To simplify the analysis, we tested their performance for the correction of low-amplitude high-order aberrations (with minimal defocus and astigmatism). Results were obtained with an AO-OCT instrument constructed at UC Davis that combines state-of-the-art Fourier-domain OCT and an AO design to allow simultaneous testing of both mirrors without the need to modify the optical system.

Keywords: Optical coherence tomography, Adaptive optics, Ophthalmology, Aberration compensation, Medical optics instrumentation

1. INTRODUCTION

Several advantages of Fourier domain OCT (FD-OCT) [1-3] over time-domain OCT have been described [4], especially for *in vivo* retinal imaging, mainly due to its significant improvement in sensitivity and acquisition speed over the standard time-domain OCT technique [5-7]. This results in fast acquisition of 3D volumetric data in clinical settings, making FD-OCT a potential tool in the future diagnosis and treatment monitoring of human retinal disease. Much of the emphasis in OCT development has emphasized improvements in axial resolution. This was made possible by the development of novel light sources, enabling axial resolution in the retina below 3 μm in both time-domain [8] and Fourier-domain systems [9-11]. In the last two years, attempts to improve lateral resolution to theoretical diffraction-limited performance has also been reported. First in the time-domain, described by Miller et al. [12] using en face coherence-gated OCT, and by Hermann et al. [13] using ultra-high resolution-OCT. For Fourier-domain OCT, Zhang et al. [14] used a line-illumination approach followed by Fernandes et al. [15] and Zawadzki et al. [16] for 3D AO-OCT. All of these reports (except [15]) used an adaptive optics system deploying a Hartmann-Shack (HS) wavefront sensor and deformable mirror for wavefront correction. This approach to improving the transverse resolution for retinal imaging has also been realized in other retinal imaging modalities [17-18].

In this paper we used a previously described hybrid AO-OCT [16] and AO-SLO [19] instrument. The AO-OCT arm combined the advantages of real-time FD-OCT and advanced technology for adaptive optics to yield in vivo imaging of 3D microscopic retinal structures.

email *rjzawadzki@ucdavis.edu; phone 1 916 734-5839; fax 1 916 734-4543; http://vsri.ucdavis.edu/

Coherence Domain Optical Methods and Optical Coherence Tomography in Biomedicine X
edited by Valery V. Tuchin, Joseph A. Izatt, James G. Fujimoto, Proc. of SPIE Vol. 6079
607908, (2006) · 1605-7422/06/$15 · doi: 10.1117/12.647568

The system has been designed to allow simultaneous testing of two deformable mirrors: a 35-element bimorph deformable mirror (DM) and a 144-element Micro-Electro-Mechanical System (MEMS) DM. These include monitoring of the subject's ocular wavefront and its Root Mean Square (RMS) error as well as comparison of the retinal OCT images acquired during testing. The latter criterion makes this approach different from evaluations concentrating on wavefronts only [20-22]. We think that testing deformable mirrors in real life situations, as the tool to improve image quality, may offer interesting insights into problems that may otherwise be overlooked by wavefront monitoring only.

2. MATERIALS AND METHODS

The optical design of the adaptive optics arm of our AO-OCT [16] system has been previously described by Laut et al. [19], except that the MEMS DM used in this work has smaller mechanical dimensions than previously reported, thus requiring small changes in the optical design to better use its active area. This has been accomplished by replacing two telescopes close to the MEMS mirror $\gamma'_{3,4} = 2.4$ and $\gamma'_{5,6} = 1.5$ by $\gamma_{3,4} = 3.2$ and $\gamma_{5,6} = 1.16$, respectively.

2.1 Experimental system

Figure 1 shows a schematic of our AO-OCT system. This system occupies 5 ft x 6 ft of a laboratory optical table. In our experiment a Superluminescent diode (840,49 nm bandwidth) was used as a light source, allowing a 6.5 µm axial resolution in the retina (n=1.38). We used a fiber-based Fourier-domain OCT instrument to optically separate sample and reference arms. A water cuvet was placed in the reference arm to compensate for eye dispersion. The detection channel of the OCT system consisted of a 100 mm focal length fiber collimator, Wasatch Photonics Holographic diffraction grating (1200 l/mm), 150 mm focal length imaging objective (air spaced triplet, Thorlabs) and a 2048 pixel Camera Link line scan CCD camera from Atmel, which allows a 2 mm axial scanning depth. Only 1024 pixels of the CCD have been used to collect spectra resulting in 512 points/A-scan sampling density after FFT. The images (B-scans) consisting of 500 A-scans or 1000 A-scans have been acquired at two different rates, 9,000 lines/s and 18,000 lines/s, resulting in frame rates of 9 Frames/s to 36 Frames/s, respectively.

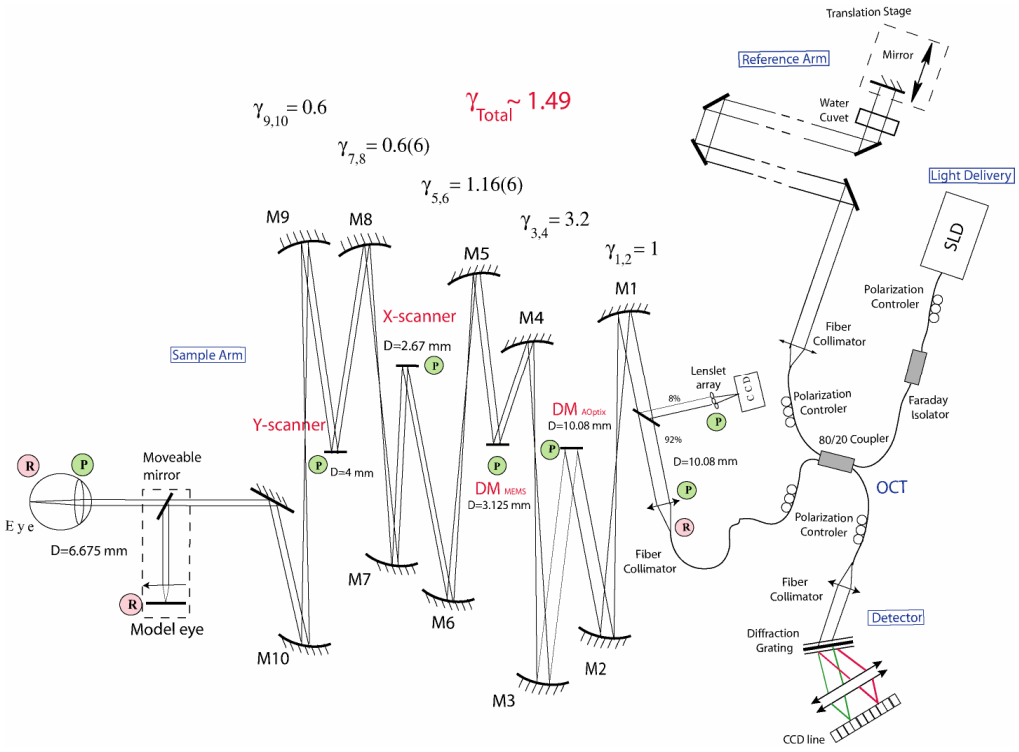

Figure 1. Schematic of AO-OCT system. Two deformable mirrors, Bimorph (AOptix) and MEMS (Boston Micromachines), are optically conjugated with the subject's eye pupil and the HS wavefront sensor. The reference arm of the AO-OCT system was designed to match the path length of the sample arm.

In the optical design of our AO-OCT instrument we used a cascade of focal telescopes (created by pairs of spherical mirrors) to produce conjugate planes of the eye pupil with all key optical components, including X and Y scanning mirrors, two wavefront correctors DM1 and DM2 and a Hartman-Shack wavefront sensor (which uses the OCT imaging light for WF reconstruction). Both DM's were placed into our AO-OCT system to allow testing of these mirrors in identical conditions, without the need to readjust any optical elements. The magnification factor, γ, between the eye pupil plane and DM planes was based upon the physical dimensions of the wavefront correctors. Accordingly, it was 1.51 for the AOptix Bimorph mirror (DM1, 10 mm diameter pupil image) and 0.47 for Boston Micromachines MEMS mirror (DM2, 3.125 mm diameter pupil image).

As pointed out in previous reports our approach differs from that described by other groups using AO-OCT because we use the OCT imaging beam to record and correct wavefront-aberrations allowing truly real-time operation of AO correction and elimination of additional light sources. Another feature of our system is the implementation of a bimorph DM to correct large amounts of defocus and astigmatism, eliminating the need for trial lenses to correct individual subject's refractive errors up to ± 3 diopters defocus and ± 1 diopter of astigmatism. The same Bimorph mirror can also be use to shift axially the focus of the AO-OCT beam to retinal layers of interest; otherwise the AO system is focused on the most scattering structures in the retina, namely on the photoreceptor/RPE layers. This is critical for AO-OCT systems as the same fiber is used for light delivery and detection; thus most of the methods used in flood illuminated AO and AO-SLO to shift focus cannot be implemented. However in this paper we will not use these functions of the bimorph mirror. The tested subject had minimal low-order aberrations, allowing deformable mirror testing for low amplitude higher-order aberration correction. Thus there was no need for trial lenses and the stroke of the MEMS and Bimorph mirror should be sufficient to flatten the wavefront.

The AO-OCT control system operates on two PC's. The schematic of this system including electrical connections is show by Figure 2. An OCT PC drives the X-Y galvo scanners and reads spectral data from the Camera link frame grabber connected to the ATMEL CCD camera. The OCT acquisition software allows real time display of the B-scans and saves the last 100 (1000 lines/Frame) or 200 frames (500 lines/Frame) depending on B-scan settings. An AO PC drives the two deformable mirrors and reads lenslet spots from the HS wavefront sensor. This computer also operates AO in a closed loop, permitting WF correction at the rate of 25 Hz. For experiments presented in this paper, however, the closed loop rate was limited to 16 Hz to increase the intensity of the spots measured by the HS wavefront sensor.

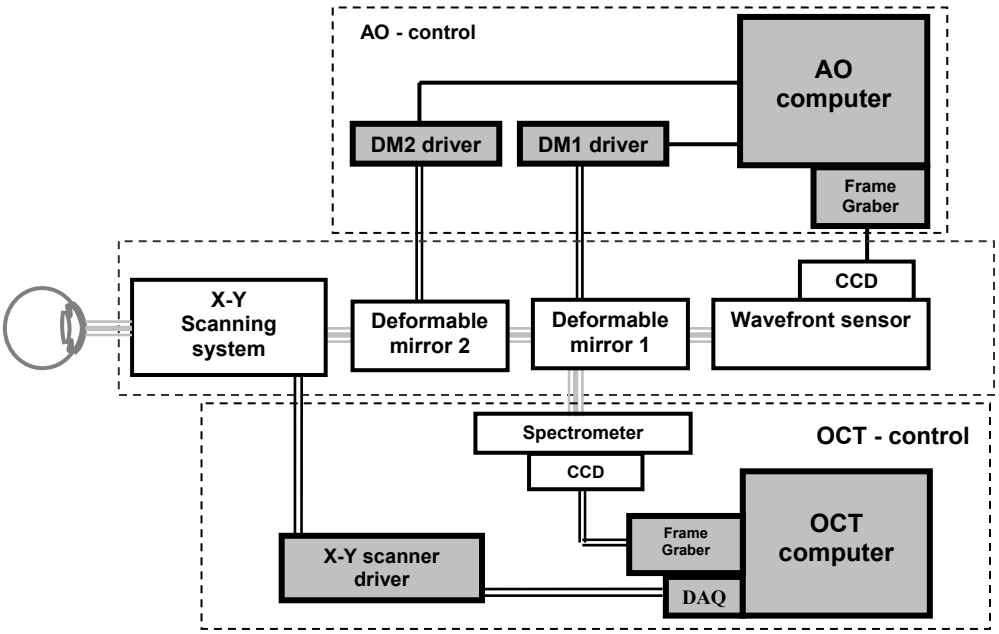

Figure 2. Schematic of the optical and electrical components of the AO-OCT system. Separate PCs were used to drive AO and OCT subsystems. Gray lines represents optical paths; Black lines represents electrical paths.

The AO closed-loop rate was the same for both deformable mirrors. During our experiments both DM's were placed in the system. Single DM AO correction was achieved by allowing only one-mirror operation at a time and by setting the

second mirror to a previously determined "flat" mode. Our AO-OCT system allows archiving of HS wavefront centroid displacements and RMS error. This was as a measure of the WF correction. The corresponding OCT images are also saved with a time-stamp for correlation with AO correction.

2.2 Adaptive Optics components

As shown by Figure 2, there are three main AO components in our AO-OCT system, two deformable mirrors and a HS wavefront sensor. Since in this paper we are concentrating on the comparative analysis of two wavefront correctors, some detailed information about key elements of our adaptive optics closed-loop system are presented.

2.2.1 AOptix Bimorph deformable mirror

The AOptics deformable mirror is a bimorph type device. Its active area is circular with a 10 mm diameter. The mirror has 35 actuators plus one guard ring and continuous surface. Interestingly, "active areas" covered by the mirror do not cover all the actuators, splitting them into two categories: 19 curvature electrodes (inner part) covered by the reflecting surface and 16 slope electrodes (outer part) separated by a guard ring. The mechanical properties of this mirror have been studied in both open- [20] and closed- [21] loop configurations. Due to the high stroke of this mirror ($\pm$ 16 μm maximum deflection, corresponding to $\pm$ 32 μm wavefront deflection), it is possible to correct for $\pm$ 3 Dpt defocus at the subject's pupil plane. Unfortunately, due to the nature of this mirror its stroke scales with the inverse square of the spatial frequency of the Zernike mode. Thus, for the highest spatial frequency mode (5 cycles/ diameter) the wavefront stroke equals 1/25 of its maximum value, namely $\pm$ 1.3 μm [23]. The mirror is operated with 15-30 V and has a response speed of about 4 kHz. Figure 3 shows the actuator geometry and a photograph of the bimorph mirror.

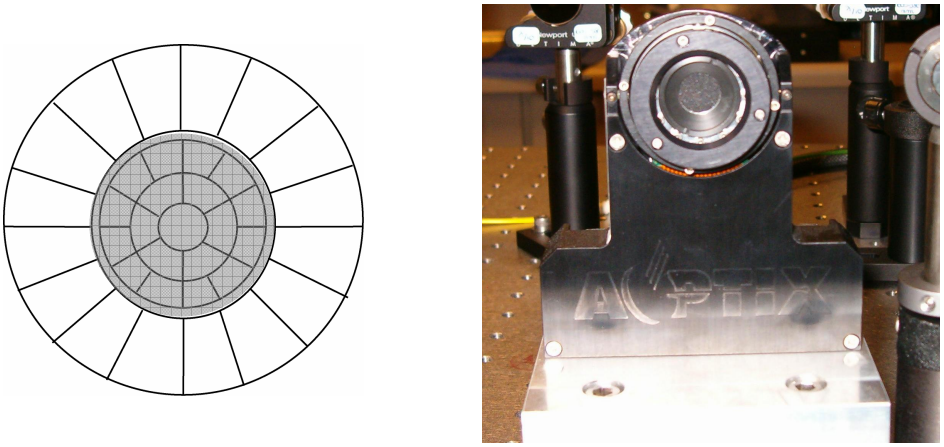

Figure 3. Actuator geometry (left) and photograph (right) for the 35-element AOptix DM. The gray area represents the image of the subject's eye pupil (diameter 6.675 mm) and has a diameter of 10.08 mm. It also corresponds to the size of the reflective surface.

2.2.2 Boston Micromachines MEMS deformable mirror

Boston Micromachines' deformable mirror is a MEMS-type device. Its active area has a square shape and covers about 3.3 mm x 3.3 mm. The mirror has 144 actuators arranged in a 12 x 12 matrix of 300 x 300 μm actuators with a continuous surface superimposed on it. Here too the "active area", covered by the reflecting surface, does not cover all the actuators. The boundary actuators are only covered by half. The mirror has a maximum mechanical deflection of $\pm$ 0.75 μm (corresponding to $\pm$ 1.5 μm wavefront deflection). Thus, for the high spatial frequency wavefront modes (5 cycles/diameter) and higher, this mirror should have better performance than the AOptix mirror. The mirror is operated at 200 V and has a response speed of about 3.5 kHz. Figure 4 shows the actuator geometry and a photograph of the MEMS mirror.

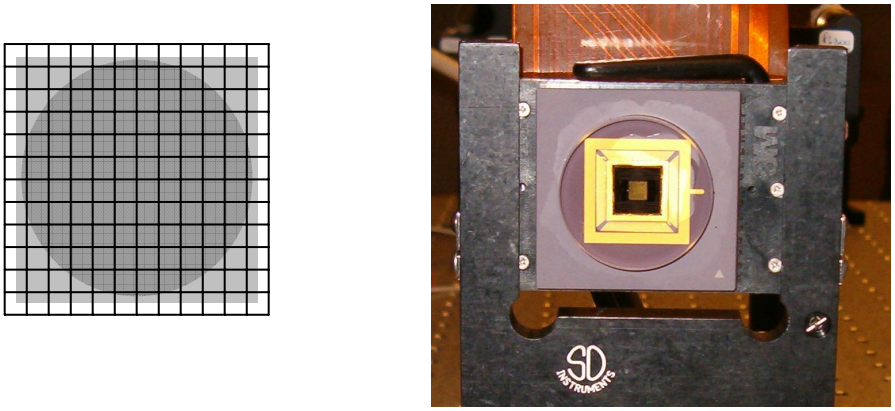

Figure 4. Actuator geometry (left) and photograph (right) for the 144-element Boston Micromachines DM. The dark gray circular area represents the image of the subject's eye pupil (diameter 6.675 mm) and has a diameter of 3.125 mm. The light gray square area corresponds to the size of the reflective surface.

2.2.2 Hartmann-Shack wavefront sensor

The Hartmann-Shack wavefront sensor is a combination of a lenslet array and a CCD camera placed in its focal plane. The sensor is a Dalsa 1M60 CCD CameraLink camera with a 20x20 lenslet array (Adaptive Optics Associates, 0500-30-S-A) having 500-μm pitch and 30 mm focal length. The circular array of the 284 lenslets, used as shown by Figure 5, is at a conjugate plane with the eye pupil and sees the 8% of the OCT light back-reflected from the retina that is redirected by a 8/92 pellicle beam-splitter. The eye pupil plane is magnified 1.49 times so that the wavefront at the pupil plane is sampled with center-to-center spacing of about 331 μm. The wavefront sensor measures centroids, i.e., displacements of the focal spots of the lenslet array from its reference position (measured for a flat wavefront during system calibration). These values are then multiplied by a control matrix that determines the array of voltages to drive the actuators of the deformable mirror. The control matrix is calculated as an inverse of the system matrix measured experimentally. Since we are using two deformable mirrors in our system this calibration step must be performed for each mirror independently. As already pointed out the HS-WS measures the WF in real time during OCT acquisition and allows closed-loop adaptive optics operation up to 25 Hz for both mirrors

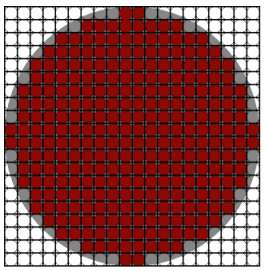

Figure 5. Lenslet geometry of our HS wavefront sensor. The gray circular area represents the image of the subject's eye pupil (diameter 6.675mm) and has a diameter of 10 mm. The dark red circles represent the position of the 284 "active" lenslets that are used during wavefront measurement.

3. RESULTS

The implication of AO correction over a 6.675 mm diameter of the eye's pupil in the diffraction-limited case would correspond to sub 3 μm lateral resolution on the retina. This, however, cannot be obtained in application and can be seen as a theoretical limit of our system performance.

During our measurement we used a bite bar and forehead rest to stabilize axial and lateral head motions for better AO correction. The eye pupil plane was carefully aligned in the system "pupil plane" by using an X-Y-Z stage connected to the bite bar and forehead rest and by monitoring the pupil image seen by the HS wavefront CCD camera. During experiments, the subject's eye was dilated and cyclopleged by Tropicamide and Cyclogel to ensure $\geq$ 7 mm pupil

size and to “freeze” subject accommodation. An external fixation target was used to help the subject maintain fixation. As previously mentioned, no trial lenses were used.

3.1 Wavefront correction

To quantitatively evaluate the ability of each DM to compensate wavefront aberration we tested the same subject and monitored wavefront and RMS error during AO correction.

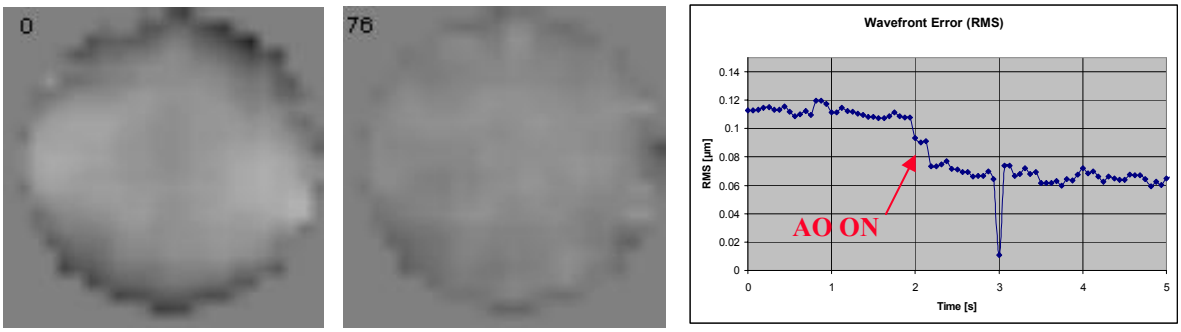

Figure 6. The ocular wavefront measured by the HS wavefront sensor before (left) and during (center) AO correction with the AOptix bimorph DM. Frame 0 is the first frame saved by the system; Frame 76 represents the wavefront measured 3.75 s after starting the archiving mode of our AO-control. Right plot shows total wavefront RMS error during AO operation. Lower values of the RMS at 3 s shows the RMS calculated during the blink.

As can be seen on that Figure the reduction of the RMS error from 0.11 to 0.06-0.065 µm was possible. Figure 7 shows the wavefront error of the same eye with correction using the Boston Micromachines MEMS DM. Here, the wavefront and RMS error have been recorded.

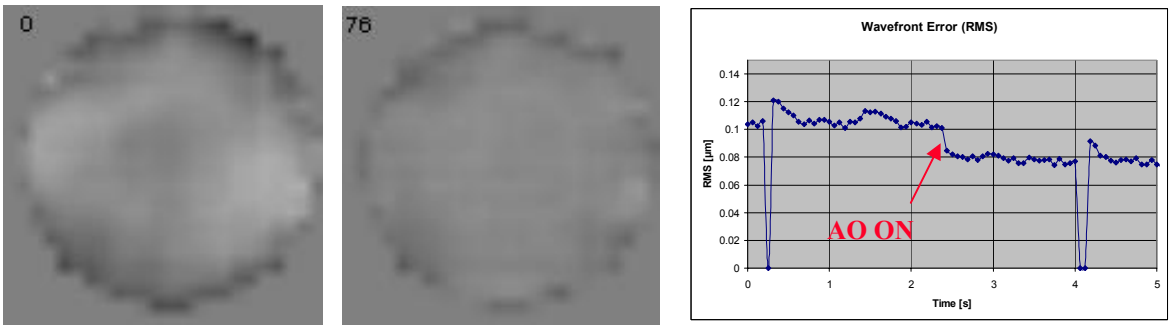

Figure 7. The ocular wavefront measured by the HS wavefront sensor before (left) and during (center) AO-correction with the Boston micromachines MEMS DM. Frame 0 is the first frame saved by the system; Frame 76 represents the wavefront measured at 3.75 s after starting the archiving mode of our AO-control. Right plot shows total wavefront RMS error during AO operation. The lower value of the RMS at 0.4 s and 4.1 s shows the RMS calculated during a blink.

These data demonstrate a reduction of the RMS error from 0.11 to 0.08 µm. Thus, in this experiment the AOptix mirror provided better correction of the higher-order aberrations.

3.2 AO-OCT retinal imaging

Retinal images were acquired with our AO-OCT system again using only one DM at a time. Figure 8 shows the results obtained with the AOptix DM correction. The OCT images obtained with the MEMS mirror for wavefront corrections are presented in Figure 9.

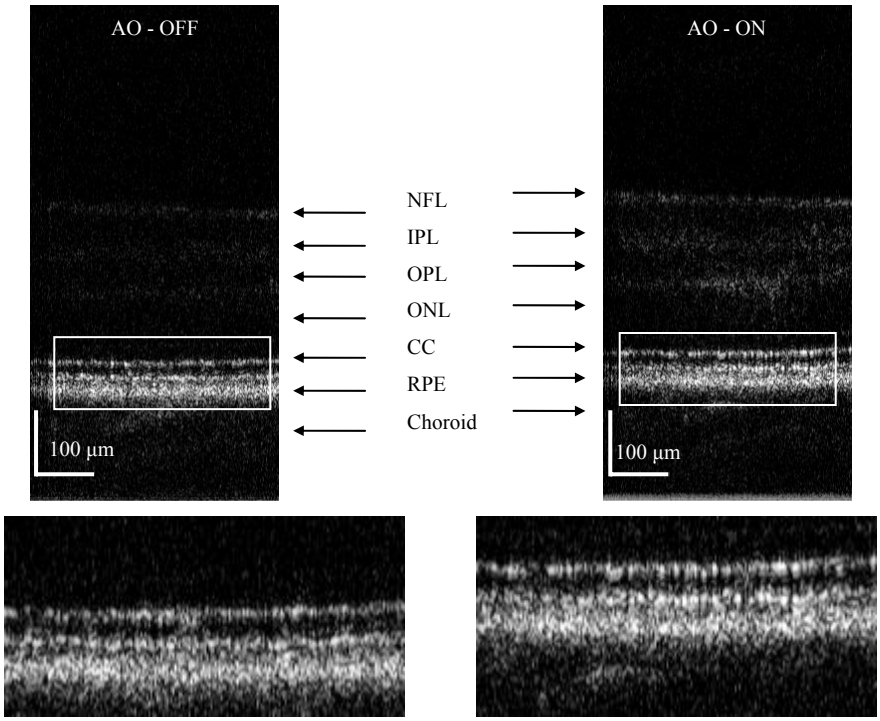

Figure 8. Upper images show B-scans acquired over 500 x1000 μm using AO-OCT implemented with the bimorph DM. Left image was obtained before AO correction and right image was obtained during AO-correction. Lower images show 2x magnification at the photoreceptor and RPE layers (100 x 400 μm). NFL – Nerve Fiber Layer; IPL – Inner Plexiform Layer, OPL – Outer Plexiform Layer, ONL – Outer Nuclear Layer, CC – Connecting Cilia, RPE – Retinal Pigmented Epithelium.

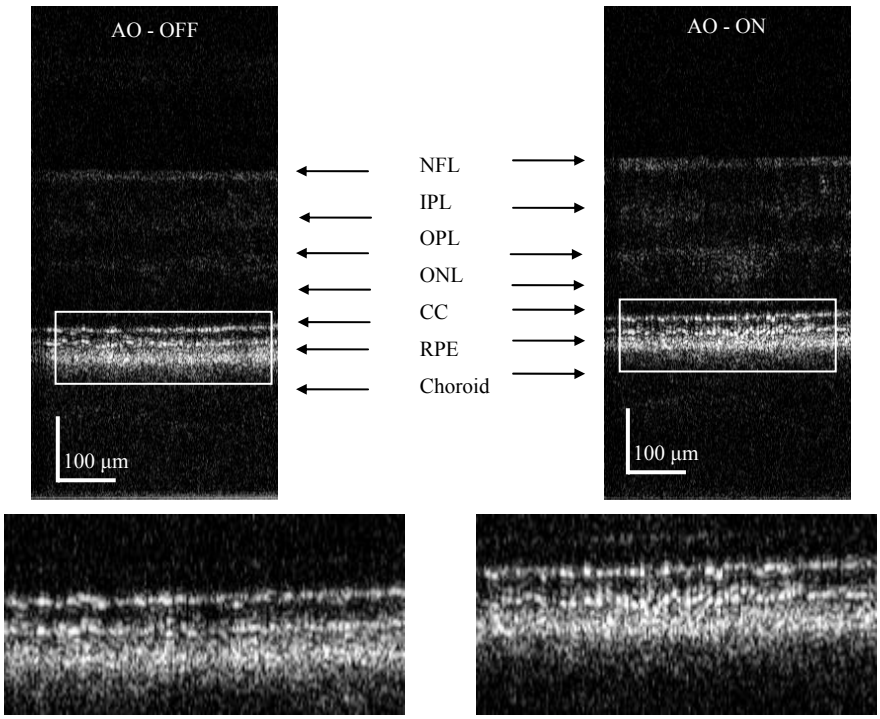

Figure 9. Upper images are B-scans acquired over 500 x 1000 μm by AO-OCT implemented with the MEMS DM. Left image was obtained before AO correction and right image was obtained during AO-correction. Lower images show 2x magnification at the photoreceptor and RPE layers (100 x 400 μm).

Interestingly, in this case the photoreceptors (at CC, corresponding to the Inner/Outer segment junctions), and Verhoeff's Membrane (RPE/Outer segment junction) can be better visualized on a B-scan although the RMS error correction was not as good as in case of the AOptix DM.

4. CONCLUSIONS

The comparative analysis of the two DMs used in our AO-OCT system shows that in presence of low amplitude high-order aberrations both mirrors have similar performance. Some discrepancies between RMS error correction and the quality of the corresponding OCT images suggest that RMS error should not be used as the only parameter describing AO system performance. The preliminary results presented in this paper have been acquired on a single subject only. Thus, further studies with more subjects will be performed.

One of the goals of this analysis was to find out if the single DM AO-OCT system with a Bimorph DM would allow sufficient wavefront correction without compromising AO performance in the high-order aberration range. These results, although promising, do not provide the answer to this question. Testing of the AOptix DM for high-order aberration correction, while it corrects low-order aberrations (defocus, coma) should be investigated in the future to fully address this problem. We will also simulate the AO-OCT system with simultaneous operation of both mirrors.

ACKNOLEDGEMENTS

We gratefully acknowledge the contributions of Donald T. Miler and Yan Zhang from the School of Optometry, Indiana University, Bloomington. This research was supported by the National Eye Institute (grant EY 014743).

REFERENCES

1. A. F. Fercher, C.K. Hitzenberger, G. Kamp, Y. Elzaiat, „Measurment of intraocular distances by backscattering spectral interferometry", Opt. Commun. **117**, 43-48 (1995)
2. M. Wojtkowski, T. Bajraszewski, P. Targowski and A. Kowalczyk „Real time in vivo imaging by high-speed spectral optical coherence tomography", Opt. Lett. **28**, 1745-1747 (2003)
3. N.A. Nassif, B. Cense, B.H. Park, M.C. Pierce, S.H. Yun, B.E. Bouma, G.J. Tearney, t.C. Chen, J,F. de Boer "In vivo high-resolution video-rate spectral-domain optical coherence tomography of the human retina and optic nerve", Opt. Express **12**, 367-376 (2004)
4. D. Huang, E. A. Swanson, C.P. lin, J.S. Schuman, W.g. Stinson, W. Chang, M.R. Flotte, K. Gregory, C.A. Puliafito, "Optical coherence tomography", Science **254**, 1178-1181 (1991)
5. J.F. de Boer, B. Cense, B.H. Park, M.C. Pierce, G.J. Tearney, and B.E. Bouma, "Improved signal-to-noise ratio in spectral-domain compared with time-domain optical coherence tomography," Opt. Lett. 28, 2067-2069 (2003).
6. R. Leitgeb, C.K. Hitzenberger, and A.F. Fercher "Performance of fourier domain vs. time domain optical coherence tomography", Opt. Express **11**, 889-894 (2003)
7. M.A. Choma, M.V. Sarunic, Ch. Yang, J.A. Izatt, "Sensitivity advantage of swept source and Fourier domain optical coherence tomography," Opt. Express 11, 2183-2189 (2003)
8. W. Drexler, U. Morgner, R.K. Ghanta, F.X. Kartner, J.S. Schuman, and J.G. Fujimoto, "Ultrahigh-resolution ophthalmic optical coherence tomography," Nature Med. 7, 502−507 (2000)
9. R. A. Leitgeb, W. Drexler, A. Unterhuber, B. Hermann, T. Bajraszewski, T. Le, A. Stingl, A. F. Fercher, "Ultrahigh resolution Fourier domain optical coherence tomography," Opt. Express 12, 2156-2165 (2004)
10. B. Cense, N.A. Nassif, T.C. Chen, M.C. Pierce, S.-H. Yun, B. H. Park, B.E. Bouma, G.J. Tearney, J.F. de Boer, "Ultrahigh-resolution high-speed retinal imaging using spectral-domain optical coherence tomography," Opt. Express 12, 2435-2447 (2004)
11. M. Wojtkowski, V.J. Srinivasan, T.H. Ko, J.G. Fujimoto, A. Kowalczyk, J.S. Duker, "Ultrahigh-resolution, high-speed, Fourier domain optical coherence tomography and methods for dispersion compensation," Opt. Express 12, 2404-2422 (2004)
12. D.T. Milller, J. Qu, R.S. Jonnal, and K. Thorn, "Coherence gating and adaptive optics in the eye" in Coherence Domain Optical Methods and Optical Coherence Tomography in Biomedicine VII, Valery V. Tuchin, Joseph A. Izatt, James G. Fujimoto, Proc. SPIE 4956, 65-72 (2003)

13. B. Hermann, E.J. Fernandez, A. Unterhubner, H. Sattmann, A.F. Fercher, and W. Drexler, P.M. Prieto and P. Artal, “Adaptive-optics ultrahigh-resolution optical coherence tomography“, Opt. Lett. **29**, 2142-2144 (2004)
14. Y. Zhang, J. Rha, R. Jonnal, and D. Miller, "Adaptive optics parallel spectral domain optical coherence tomography for imaging the living retina," Opt. Express **13**, 4792-4811 (2005)
15. E. Fernández, B. Povazay, B. Hermann, A. Unterhuber, H. Sattman, P. Prieto, R. Leitgeb, P. Anhelt, P. Artal, W. Drexler, "Three-dimensional adaptive optics ultrahigh-resolution optical coherence tomography using liquid crystal spatial light modulator" Vis. Research **45**, 3432-3444 (2005)
16. R. Zawadzki, S. Jones, S. Olivier, M. Zhao, B. Bower, J. Izatt, S. Choi, S. Laut, and J. Werner, "Adaptive-optics optical coherence tomography for high-resolution and high-speed 3D retinal in vivo imaging," Opt. Express **13**, 8532-8546 (2005)
17. J. Liang, D.R. Williams and D.T. Miller, “Supernormal vision and high-resolution retinal imaging through adaptive optics“, J. Opt. Soc. Am. A **14**, 2884 (1997)
18. A. Roorda, F. Romero-Borja, W.J. Donnelly III, H. Queener, T.J. Hebert, and M.C.W. Campbell, “Adaptive optics scanning laser ophthalmoscopy“, Opt. Express **10**, 405-412 (2002)
19. S.P. Laut, S.M. Jones, S.S. Olivier, and J.S. Werner, “Scanning laser ophthalmoscope design with adaptive optics” in Smart Medical and Biomedical Sensor Technology III; Brian M. Cullum, J. Chance Carter, Proc. SPIE, 6007, (2005)
20. D.A. Horsley, H. Park, S.P. Laut, and J.S. Werner, “Characterization for vision science applications of a bimorph deformable mirror using phase-shifting interferometry” in Ophthalmic Technologies XV, Fabrice Manns, Per G. Soederberg, Arthur Ho, Bruce E. Stuck, Michael Belkin, Proc. SPIE, 5688, 133-144 (2005)
21. S. Laut, S. Jones, H. Park, D.A. Horsley, S. Olivier, and J.S. Werner, “Bimorph deformable mirror: an appropriate wavefront corrector for retinal imaging?” in Smart Medical and Biomedical Sensor Technology III; Brian M. Cullum, J. Chance Carter, Proc. SPIE, 6007, (2005)
22. E. Dalimier and C. Dainty, "Comparative analysis of deformable mirrors for ocular adaptive optics," Opt. Express **13**, 4275-4285 (2005)
23. AOptix Technologies, Inc, “High stroke standalone deformable mirror (SDM) user manual”